JOURNAL OF GUIDANCE, CONTROL, AND DYNAMICS
Vol. 16, No. 5, September–October 1993

Gain Adaptive Tracking

D. D. Sworder*
University of California, San Diego, La Jolla, California 92093
R. Vojak†
INRIA, Rocquencourt, France
and
R. G. Hutchins‡
ORINCON Corporation, San Diego, California 92121

Properly joining the different modes of a multiregime tracker is difficult. This paper describes a novel, image-based algorithm for tracking a maneuvering target. The form of the algorithm is like the extended Kalman filter, but the gain adjustment utilizes image information in a sophisticated manner to better compute the error covariance. The performance of this filter is compared with two alternatives: an extended Kalman filter without image augmentation and an extended Kalman filter with acceleration aiding and simple, image-derived gain scheduling. The response of the proposed tracker is shown by example to be superior to the others. Although too complex to permit online implementation, the performance of the algorithm provides a useful bound on tracker fidelity attainable with an image-augmented architecture.

Introduction

A TRACKING algorithm is a causal mapping from a spatiotemporal observation to an estimate of the dynamic state of a target. Perhaps the most widely studied model-based tracking algorithms are the Kalman filter and its lineal variants. The dynamic features of the target are represented by a state process $\{x_t\}$ having as components positions, velocities, and perhaps accelerations in an appropriate reference frame. The observation process $\{y_t\}$ is derived from a radar or a similar device that provides a measurement—albeit a noisy one—of the location of the target, e.g., range and bearing. In this modeling paradigm, the quantities that appear in the state vector are closely interlinked with the observation in the sense that measured properties of the target are directly reflected in the equations of dynamic evolution and unmeasured ones are ignored. This oft neglected linkage between the sensor suite and the state space model is clearly seen in the orthodox motion model. When the sensor measures the attributes of a point-equivalent object, not coincidentally, the state space consists of the point properties of the target. Other relevant but unmeasured variables, e.g., target orientation, are not included in the target dynamics. In this sense, the sensor suite has a major role in determining the breadth of the state space model; new sensors "create" new components in the state space.

Linear differential (or difference) equations with additive random forcing terms are used in most analytical studies to delineate the motion dynamics[4]

$$\mathrm{d}x_t = A_t x_t\,\mathrm{d}t + \mathrm{d}w_t \tag{1}$$

with the observation given at discrete times by a linear function of the state.

$$\begin{aligned} y_t &= Dx_t + n_t \qquad \text{at observation times} \\ &= 0 \qquad\qquad\quad \text{otherwise} \end{aligned} \tag{2}$$

[Equations (1) and (2) model an environment with continuous time dynamics and discrete time observations. Similar conclusions are obtained when either is replaced by a proper analog.] In this model, $\{w_t\}$ is a vector Brownian motion process with intensity W ($\mathrm{d}w\,\mathrm{d}w' = W\,\mathrm{d}t$), and $\{n_t\}$ is a Gaussian "white noise" sequence with covariance $R_x > 0$, independent of $\{w_t\}$ and the initial condition on Eq. (1). Equation (1) is written in terms of differentials: stochastic and deterministic. In many cases, this level of abstraction is unnecessary; the equation can be formally divided by $\mathrm{d}t$ and the result expressed as an ordinary differential equation with a white noise excitation (see Ref. 1, Chap. 4). This more traditional formalism gives considerable insight into the issues of estimation and leads directly to the Kalman filter. However, when it is necessary to study systems that contain essential nonlinearities, or that are subject to sudden and unpredictable changes, it is expedient to retain the flexibility resident in Eq. (1).[2]

If the initial conditions are suitably selected, Eqs. (1) and (2) delineate the classical linear Gauss-Markov (LGM) model. In many applications, the relations between the indicated variables are nonlinear, e.g., range and bearing are nonlinear functions of the target location expressed in the usual Euclidian $\Re^3$ space. If the nonlinearity is smooth, it is possible to linearize it about the estimated state, and a quasi-LGM model results; e.g., the gradient of the observation mapping replaces the D matrix in Eq. (2). If the linear (or linearized) equations provide an adequate description of the signal and the observation and their interconnection, there is a well-known solution to the mean-square inference problem—the (extended) Kalman filter (EKF). Denote the information pattern (filtration) generated by the sensor measurements by $\{Y_t\}$. The best mean-square estimate of the state is given by the Y_t conditional mean of x_t [$\hat{x}_t = E(x_t \mid Y_t)$] where between observations

$$\frac{\mathrm{d}}{\mathrm{d}t}\hat{x}_t = A_t\hat{x}_t \tag{3a}$$

and at an observation time

$$\Delta\hat{x}_t = P_{xx}D'(DP_{xx}D' + R_x)^{-1}\Delta\nu_x \tag{3b}$$

with (the increment of the innovations process) $\Delta\nu_x = y_t - D\hat{x}_t$ at the observation times and zero elsewhere, and P_{xx} the error covariance matrix. (For any piecewise continuous process, let

Received Jan. 25, 1992; revision received Oct. 23, 1992; accepted for publication Oct. 26, 1992.

*Professor, Department of Electrical and Computer Engineering.
†Research Associate.
‡Principal Engineer.

$\Delta z_t = z_{t+} - z_{t-}$. Then Δz_t is zero where $\{z_t\}$ is continuous and gives the jumps in $\{z_t\}$ at points of discontinuity.) The appearance of Eq. (3) is common in applications. It has a suggestive form that transcends the fact that it was derived under the LGM hypothesis. The increment $\{\hat{x}_t\}$ is expressed as a sum of an extrapolation (3a) and a correction (3b). The former is determined by the direction of the mean state increment, and the latter is proportional to the increment in the innovations process. The correction has a gain factor related to the residual uncertainty in the estimate (P_{xx}). Only this factor is not given explicitly in the model of the observation link, and indeed P_{xx} is determined jointly by the target dynamics and observation fidelity.

The error covariance acts to adapt the weight accorded to new information to fit current circumstances. When P_{xx} is small—little estimation uncertainty—the innovations process is of little note, and the estimate propagates forward along the field of the unexcited system. As the uncertainty in the state estimates increases, new information is accorded increasing value; i.e., as the estimator becomes less sure of the true state, it is more willing to modify its prior estimate in response to new data. It is well known that $\{P_{xx}\}$ is given by the solution to a matrix ordinary differential equation between observations, with jumps at the observation times: between observations

$$\frac{\mathrm{d}}{\mathrm{d}t}P_{xx} = AP_{xx} + P_{xx}A' + W \tag{4a}$$

and at an observation time

$$\Delta P_{xx} = -P_{xx}D'(DP_{xx}D' + R_x)^{-1}DP_{xx} \tag{4b}$$

subject to appropriate initial conditions. The error covariance is contingent on the intensity of the exogenous processes in both state and observation; e.g., as W increases, the increment in $\{P_{xx}\}$ increases as well. This has an intuitive justification. As the state process becomes more volatile, P_{xx} increases, and through this intermediary, the EKF becomes "faster" and more responsive to state changes. Of course, as a corollary to this, the same filter will amplify the measurement noise $\{n_t\}$. To distinguish this estimator from those that follow, and to emphasize its dependence on W, Eqs. (3) and (4) will be called the EKF_W algorithm.

Equations (3) and (4) and their discrete time analogs have been studied intensively, and the approach just outlined has been used in numerous applications. At first glance, this outcome might be surprising since there are few circumstances in which the LGM model is strictly valid. However, one of the attractive properties of the EKF_W is its generalized robustness; even if the actual environment differs slightly from that described in Eqs. (1) and (2), Eq. (3) gives a "good" estimate of the state (Ref. 3, Chap. 6). "Slight" depends on the context, of course, but streamlined models frequently lead to satisfactory estimators, an appealing prospect when the computational load on the processors is burdensome, and the designer seeks to reduce the filter dimension as much as is practical. There is considerable flexibility in structuring the external disturbances. By proper filtering and shaping, the exogenous processes $\{w_t\}$ and $\{n_t\}$ can be used to portray a wide range of phenomena including such seemingly disparate sources of excitation as pilot-induced maneuvers and aerodynamic turbulence. Many examples are found in textbooks such as Maybeck's comprehensive three-volume work.[4] Maybeck shows clearly that sophisticated use of the degrees of freedom in the predictor-corrector framework delineated by Eqs. (3) and (4) creates serviceable solutions to numerous and seemingly unrelated estimation problems.

The issues that arise in tracking become clearer when discussed in the context of a specific example. Although the detailed conclusions are application particular, the essential structure of the estimation synthesis procedure has general relevance. Consider the problem of tracking the motion of an agile object in the X-Y plane. A simple model for an evasive target moving at essentially constant speed is given by the fourth-order equation

$$\mathrm{d}\begin{bmatrix} X \\ Y \\ V_x \\ V_y \end{bmatrix} = \begin{bmatrix} 0 & 0 & 1 & 0 \\ 0 & 0 & 0 & 1 \\ 0 & 0 & 0 & -\omega_\psi \\ 0 & 0 & \omega_\psi & 0 \end{bmatrix} \begin{bmatrix} X \\ Y \\ V_x \\ V_y \end{bmatrix} \mathrm{d}t + \begin{bmatrix} 0 & 0 \\ 0 & 0 \\ 1 & 0 \\ 0 & 1 \end{bmatrix} \mathrm{d}\begin{bmatrix} w_x \\ w_y \end{bmatrix} \tag{5}$$

where $\{X_t, Y_t\}$ are position coordinates, and $\{V_x, V_y\}$ are associated velocities. The target is subject to two types of acceleration: a wide-band omnidirectional acceleration described by the Brownian motion $\{w_x, w_y\}$, and a maneuver acceleration represented by the turn rate process $\{\omega_\psi\}$. The former fits well within the LGM framework [see Eq. (1)], but the latter is troublesome in two respects. First, because of their temporal structure, the sample paths of the maneuver accelerations are better described by a discontinuous rather than a continuous process and are clearly non-Gaussian (see Ref. 5 and the references therein). Second, the target dynamics are indexed by the turn rate and are consequently polymorphic (PM). Treating the maneuver as an additive disturbance neglects the strict coupling between the direction of the acceleration and the velocity vector. In volatile encounters, the lateral acceleration is the primary one, thus making the conventional formalism of doubtful applicability.[6]

The maneuvering target problem has received considerable attention in the literature where it is usually assumed that estimation and prediction are accomplished using bearing and perhaps range data. The simplest estimators use an EKF_W derived by neglecting the turn rate process, or by augmenting W to account for its power (adding pseudonoise). The first of these options is very optimistic in so far as the computed error covariance process is far too small. If the two options are blended, the tracker could be designed "under the assumption that the target acceleration is constant . . . while providing a high enough bandwidth to adequately track target acceleration changes when they occur. However, one of the principal drawbacks to this approach is that a high bandwidth filter may not attenuate the noise present in the system."[7] The exigencies created by the need for high-accuracy tracking during quiescent operation must be balanced against the possibility of large errors and loss of lock during turns, and with the single degree of freedom found in EKF_W, this balance will be difficult to achieve. There is also the option of replacing the maneuver process by a Gaussian process generated by "shaping" white noise. This has proven effective in certain cases, but requires careful tuning.[8] The EKF_W in this case is based on a model with fixed parametric form [or monomorphic (MM) model].

Alternatively, the PM models represent target motion with a family of equations, each tuned to a different turn rate hypothesis. If the maneuvers could be detected expeditiously, the encounter model would be linear, albeit time variable. The associated EKF would simply be given by Eqs. (3) and (4) with A_t changing concurrently with the maneuver. When the observations are equivocal, a set of estimators could be associated with the individuated models and operated in parallel. The outputs of these filters could then be combined to give the location estimate (see Ref. 9, for example). If the proper model changes with time in an unpredictable manner, there are an infinite number of distinct path hypotheses that must be accounted for in the PM algorithm. Novel methods of information transfer between the parallel filters have been proposed to achieve accurate tracking, leading to robust performance in many cases. The most promising of these, the interacting multiple model (IMM) method of Blom and Bar-Shalom, has received considerable attention in this application.[10-13]

Estimators have become increasingly sophisticated as more versatile online processors have become available. For example, in some trackers a forward-looking infrared (FLIR) sen-

sor generates a sequence of pictures of the target as it moves within surroundings containing significant clutter. From these data frames, the target pixels are localized, and important spatial properties are deduced with an image processor. For example, target type and angular orientation with respect to the sensor can be obtained from an analysis of the ostensible shape. In Ref. 14 this problem was considered, and motivated by the availability of an online imaging capability, the estimation architecture shown in Fig. 1 was explored. The tracker makes use of two data paths. The lower one is a conventional mapping of center-of-reflection data into an estimate of target location; i.e., it accomplishes the $\{y_t\}$ to $\{\hat{x}_t\}$ transformation. The upper path is image specific, mapping a sequence of image processor outputs into a signal (indicated here by $\{\hat{\alpha}_t\}$), which is used to adjust the tracker to changing conditions. This explicit dependence on $\{\hat{\alpha}_t\}$ renders the tracker adaptive.

To understand how the designer can best avail himself of the information in the upper path, note that the imager is a natural complement to a range-bearing sensor, providing spatially extended features rather than the location of a point-equivalent target. Figure 2 shows a sequence of images of an F-14 as it rolls. These data frames were created in infrared at a rate of 30 frames/s at the Point Magu Naval Air Station and are displayed here as visible duplicates. The target images were taken from the Image Processing for the Identification of Non-Cooperative Targets (IMPRINT) data base created by the Hughes Aircraft Company under the sponsorship of the Naval Air Development Center in Warminster, Pennsylvania. For a subset of the IMPRINT imagery, target orientation coordinates were recorded concurrently from an onboard inertial navigation system (INS). These INS measurements were used to evaluate errors accruing to the image interpretation procedure. Figure 2 shows the silhouette selected by the image processing algorithm overlaid on the target image. When there are many pixels on target classification is quite good, but there are major errors when the target subtends a small angular region of the focal plane.

In the tracking application, the imager creates a data sequence $\{z_t\}$ that is discrete in both time and space. Time quantization is not unusual [see Eq. (2)], but spatial quantization is unorthodox. The imager generates a set of statements about target status rather than generating a measurement whose natural range is an interval. The image processor translates a data frame into a statement of category selected from a prespecified alphabet of topical symbols. Over time, a sequence of these symbols is generated. Some of the symbols correctly describe the target, and some do not. As with the usual estimation procedures, the underlying mathematical model is to be used to help interpret this discrete sequence to best advantage. This is a far from trivial problem because of the complex dynamic phenomena that are represented by the model.

To integrate the image information into an estimation algorithm like the EKF, the encounter model must be completed. There are two accelerations influencing the target path in Eq. (5)—the omnidirectional process $\{w_t\}$ and the turning process. Because the turn rate tends to be nearly constant over intervals, with sudden changes at unpredictable times, a useful model is created by partitioning the range of turn rates into K levels that is, $\omega_\psi \in \{a_1, \ldots, a_K\}$.[15,16] The indicated acceleration states are aggregates in so far as the actual acceleration is randomly placed within the associated bin. For notational convenience, it is advantageous to replace the multivalued process $\{\omega_\psi\}$ with a process taking on values in a set of unit vectors. Let $\{\alpha_t\}$ be the maneuver indicator process, $\alpha_t = \boldsymbol{e}_i$ if $\omega_\psi = a_i$ at time t. [Let $\boldsymbol{e}_i$ be a unit vector with a one in the ith component. To simplify the notation when dealing with indicator processes like $\{\alpha_t\}$, an integer subscript will denote the component of the vector rather than the value of the vector at a particular time; e.g., α_1 is to be understood as (the scalar) $(\alpha_t)_1$, the first component of the vector α_t.]

To complete the motion model, the dynamics of the maneuver process must be quantified. The most common way to do this is to suppose the successive maneuver modes are represented by a Markov chain with transition rate matrix q. (See Ref. 17, p. 641 for a discussion of this matrix. If $i \neq j$, the matrix element q_{ij} is the transition probability rate from maneuver mode i to maneuver mode j. The diagonal elements are determined by normalization.) This is a tractable model, the parameters of which can be expressed in terms of the mean lifetime of each maneuver mode, and the transition probabilities between modes. This analytical description of tempo subsumes the case in which the turn rate is an unknown constant,[18] and has been proposed to describe the temporal dynamics of pilot induced acceleration.[5]

Although modeling the turn rate in this way makes analysis more difficult because it leads to non-Gaussian sample paths in Eq. (5), certain conceptual advantages accrue to the assumption that the maneuver acceleration is piecewise constant. Equation (5) is a linear equation with an unknown maneuver parameter α_t. This fact suggests that estimation could be divided into distinct phases. First, the maneuver is detected. Second, the Kalman filter state is corrected to compensate for residual errors from the previous maneuver, and finally, after detection and correction, the Kalman filter parameters are adjusted in anticipation of future maneuvers.[19] Although intuitively appealing, there are difficulties with this seemingly self-evident procedure. It was noted by Williams and Friedland[7] that the covariance of the tracker must be reset to reflect the increased uncertainty in the maneuver estimation near the time of a transition. To quantify this uncertainty is difficult. The uncertainty increases in the interval between a transition and its detection, but $\{P_{xx}\}$ as given in Eq. (4) does not reflect this.

In this paper, a new image-based algorithm is presented that addresses these fundamental issues. The image path shown in Fig. 1 is used to generate the information needed to achieve the required gain adjustment. In this manner, a tracker is produced that has wide bandwidth during volatile conditions and a narrower one during quiescent intervals. The advantage of using the imager outputs in this way is that they give a much quicker indication of a change in the encounter than is provided by the path estimates alone. Proper use of the image path in Fig. 1 permits the covariance-reset problem discussed by Williams and Friedland[7] to be resolved.

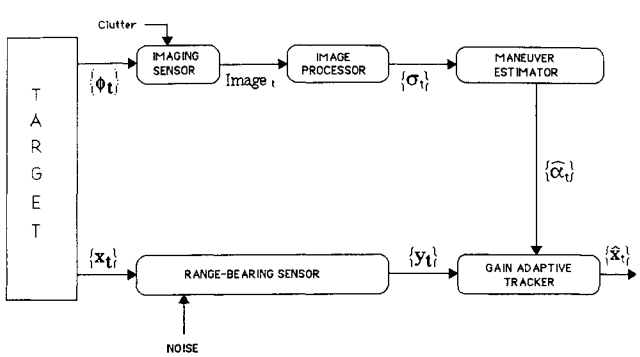

Fig. 1 Image-enhanced tracking architecture.

Image-Enhanced Estimation

The advantages of the dual path architecture were noted by Maybeck and his coworkers (see, for example, Ref. 14). In an important series of papers, Andrisani and his coworkers studied this problem within the EKF framework. Angular orientation is clearly relevant to target tracking, and for this reason angular variables were added to the state space model in Refs. 20 and 21. The measurement equation used in the references mimicked Eq. (2); i.e., the center-of-reflection and the angular variables were both measured with an additive, white noise channel. The authors observed that "attitude information, obtained from an optical image processor, in a tracker's

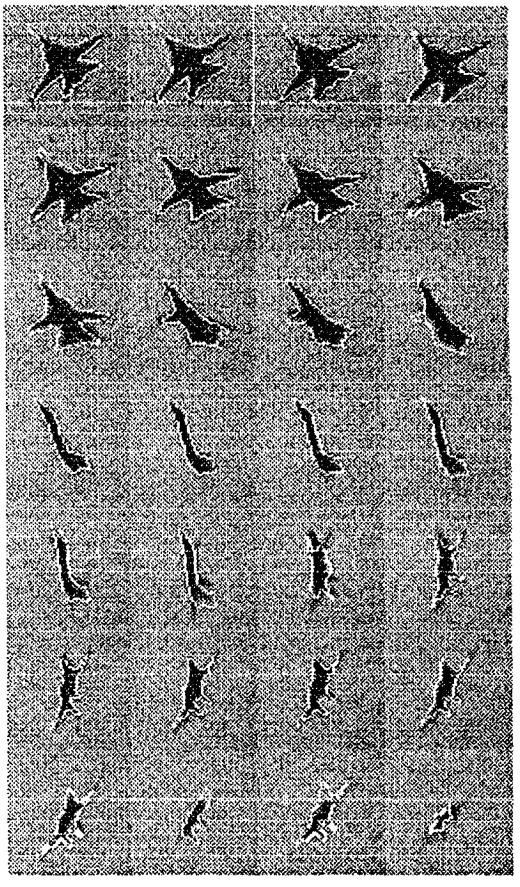

Fig. 2 Imagery of a maneuvering F-14.

Kalman filter gives valuable lead information when tracking a fixed wing aircraft by being able to determine the direction of the lift vector."[22] The "lead" in the image data is of fundamental importance in improved tracker performance. Position is two integrals removed from an acceleration. A maneuver manifests itself in a path change over time, but initially this change is difficult to detect in the noisy location data available to the tracker. Orientation is a much faster indicator. After factoring in geometric effects, a change in orientation of a fixed wing aircraft gives an immediate indication of a maneuver, and this can be used to adjust the gains in the EKF. For a target such as a tank, a jinking path is created by turning, and the turn rate can be deduced from changes in angular orientation. In both cases, direct measurement of target orientation gives a faster indication of a maneuver than could be obtained from noisy trajectory data alone. In a novel study of the utility of augmented sensor systems, Lefas[23] noted that if the roll angle were transmitted from the target to the tracker, improved performance would be attainable using a roll-angle adaptive filter. The problem that motivated his analysis involved estimating the trajectory of a cooperative target (air traffic control), and attention was focused on adaptive MM filters in which the gain is adjusted whenever a maneuver is suspected. Although the resulting architecture would not be suitable in a hostile engagement, his results illustrate the usefulness of maneuver-adaptive estimation for tracking agile targets.

To synthesize an image-enhanced tracker, a suitable analog to Eq. (2) must first be constructed. The imager is a feature matching block, and its errors are not well described by additive Gaussian noise. To create a more realistic model of the orientation classifier, suppose that the imager collects data at a rate of λ frames/s and places each target image into one of L equally spaced orientation bins. The output of the processor can be written as an L-dimensional counting process $\{\sigma_t\}$, the ith component of which is the number of times the target has been placed in bin i on the interval $[0, t]$. This sequence of counts (or symbols) can be interpreted by a temporal processor to give the relative likelihoods of the various turn rate hypotheses. This development can be summarized as follows. Let the orientation indicator process be given by $\{\rho_t\}$; $\rho_t = \boldsymbol{e}_i$ if the current target orientation is in the ith bin. The composite maneuver status of the target is given by $\{\phi_t\} = \{\alpha_t \otimes \rho_t\}$, the Kronecker product of maneuver and orientation.[24] [The Kronecker product of a $p \times q$ matrix A and an $m \times n$ matrix B is a $pm \times qn$ matrix $A \otimes B$ defined in blocks of size $m \times n$ by $(A \otimes B)_{ij} = a_{ij}B$. For example, if α and ρ are $(1 \times K)$ and $(1 \times L)$, respectively, the vector $\phi = \alpha \otimes \rho$ is $(1 \times KL)$, with elements $(\alpha_1\rho_1, \alpha_1\rho_2, \ldots, \alpha_1\rho_L, \alpha_2\rho_1, \ldots, \alpha_K\rho_L)$. Since both α and ρ are unit vectors, ϕ must be a unit vector as well; albeit in a higher dimensional space. The nonzero (unit) element of ϕ delineates both the maneuver regime and the target orientation; e.g., if $\phi_1 = 1$, then necessarily $\alpha = \boldsymbol{e}_1$ and $\rho = \boldsymbol{e}_1$. Both α and ρ are easily extracted from ϕ. Let $\boldsymbol{I}_r$ be an r-dimensional identity, and let $\boldsymbol{1}_s$ be an s-dimensional vector of ones. The matrix $(\boldsymbol{I}_k \otimes \boldsymbol{1}_l')$ is $(K \times KL)$, and direct evaluation yields the identity $(\boldsymbol{I}_k \otimes \boldsymbol{1}_L')\phi = \alpha$. Similarly $(\boldsymbol{1}_K' \otimes \boldsymbol{I}_L)\phi = \rho$.] The quality of image interpretation is determined by the $L \times L$ discernibility matrix $\boldsymbol{P} = [\boldsymbol{P}_{ij}]$ where $\boldsymbol{P}_{ij}$ is the probability that bin i will be selected by the processor if bin j contains the true target orientation at time of image creation[25]

$$\boldsymbol{P}_{ij} = \mathcal{P}(\Delta\sigma_i = 1 \mid \rho = e_j) \tag{6}$$

The fidelity of image interpretation is a function of three things: the frame rate λ, the ability of the image to correctly classify a single image $\boldsymbol{P}$, and the tempo of the encounter q. These factors interact in subtle ways. For example, a rapid tempo requires a high frame if expeditious maneuver detection is to be accomplished. In the same way, to compensate for a low frame rate, the quantization must be fine (L large) and the processing accurate ($\boldsymbol{P} \cong \boldsymbol{I}$). The comprehensive orientation dynamics of the target can be described by a $KL \times KL$ dimensional transition rate matrix Q, which depends on the generator of the acceleration chain, and the generator of the random angular motions for a given acceleration. Because the imager measures directly the target features that most clearly manifest changes when the target turns, the image-based path gives a much more expeditious indication of a maneuver than does the lower path. There is little error, therefore, if turn rate estimation is based exclusively on image data; i.e., rather than detecting a maneuver from both orientation changes and path deviation, only the former is used. Denote the information pattern generated by $\{\sigma_t\}$ by $\{Z_t\}$. The conditional probabilities of the various turn rate hypotheses are given by the K-dimensional process $\{\hat{\alpha}_t\}$

$$\hat{\alpha}_t = [\mathcal{P}\{\omega_\psi = a_i \mid Z_t\}] \tag{7}$$

$$= (\boldsymbol{I}_K \otimes \boldsymbol{1}_L')\hat{\phi}_t \tag{8}$$

The operator $(\boldsymbol{I}_K \otimes \boldsymbol{1}_L')$ extracts the components of the maneuver estimate from the estimate of the modal state. (A similar equation could be written for generating $\hat{\rho}_t$, if required.)

The upper link in Fig. 1 generates $\{\hat{\phi}_t\}$ and uses Eq. (8) to determine the likelihood of the various maneuver hypotheses. To gain insight into its operation, note that the image data are reduced in the image processor to a counting process $\{\sigma_t\}$. The increment in $\{\sigma_t\}$ is the zero vector between observations, and a unit vector at an observation time; e.g., $\Delta\sigma_t = \boldsymbol{e}_i$ indicates that the ith symbol was received at time t. Consider a simple situation in which $\boldsymbol{P} \cong \boldsymbol{I}$, and the true target orientation is in the first bin for an interval. In this case, one would expect a sequence of measurements $\Delta\sigma_t = \boldsymbol{e}_1$ with rate λ; i.e., the observation string $\{1, 1, 1, 1, 1, \ldots\}$ is compatible with a "coasting" (or nonturning) hypothesis. Suppose the observation string were modified; e.g., $\{1, 1, 1, 1, 2, \ldots\}$. The receipt of the symbol 2 has two effects. First, the rate of occurrence of symbol 1 is now less than λ, and this should be

judged as a failure to reconfirm hypothesis number one. Second, the rate of symbol 2 now becomes positive. Of course, this anomalous symbol could be a false indication of angular change, or it could be symptomatic of a turn.

Figure 3 shows the output of the image processor for a coast-turn-coast maneuver to be studied in more detail in the next section. The orientation bins are 30 deg wide; $L = 12$. Suppose that there are many pixels on target, but there is an aliasing in the image processor because image classification is strongly based on the seeming silhouette. Silhouette is an ambiguous feature, the same for both the true orientation and another symmetrically placed with respect to a line perpendicular to the line of sight. In the figure, the ordinate is bin number as classified by the image processor (the component of $\Delta\sigma$ equal to 1), and the abscissa is time. With a 10 frames/s imager, the dwell in each bin is unrecognizable in the graph, but the curve in an expanded scale would be piecewise constant. Note that the image errors create an unconventional data sequence. The coasting phase ($t < 10$ s), which has an essentially constant angular process ($\rho_r \equiv e_1$), displays considerable volatility in the angular measurement; image aliasing ($\Delta\sigma = e_7$) masks the true path. The actual angular path would have a constant slope during the turn, but the orientation must cross a bin boundary before a change is recognized at the output of the image processor. When the target exits bin 4 ($t \cong 15$ s), is it continuing the turn, reversing the turn (recall the frequency of angular aliasing), or coasting? Each hypothesis is compatible to some degree with $\{\sigma_t\}$. A robust procedure for image interpretation is required if the upper path in Fig. 1 is to be useful in tracking and prediction.

The basic angular information is contained in the rate of image symbol occurrence. To be more specific, consider an L-dimensional, piecewise constant process with jumps at the image observation times

$$\{(\Delta\vartheta_t)_j\} = \{\lambda \textstyle\sum_k \boldsymbol{P}_{kj} \hat{\lambda}_k^{-1} \Delta\sigma_k\}$$

This process is important to image interpretation, and it is good to have a clear sense of what it signifies. Note that $\boldsymbol{P}_{ij} = \mathcal{P}(\Delta\sigma_i = 1 \mid \rho = \boldsymbol{e}_j)$, and so $\Delta\vartheta_j = \lambda\hat{\lambda}_i^{-1}\mathcal{P}(\Delta\sigma_i = 1 \mid \rho = \boldsymbol{e}_j)$. Suppose symbol i is observed at time t ($\Delta\sigma_i = 1$). If the expected rate of the ith symbol is small, and the ith symbol is received, the unnormalized weighting of the jth angular hypothesis, $\mathcal{P}(\Delta\sigma_i = 1 \mid \rho = \boldsymbol{e}_j)$, is increased by the factor $\lambda\hat{\lambda}_1^{-1}$. This weighting on an unanticipated symbol will be quite big if it actually occurs. Alternatively, if the ith symbol were expected, i.e., if $\lambda \cong \hat{\lambda}_i$, and symbol i does indeed occur, then the increment in $\{\vartheta_j\}$ is approximately the unnormalized discernibility coefficient $\boldsymbol{P}_{ij}$. Unforeseen events are given amplified in $\{\vartheta_t\}$ more than confirming events are.

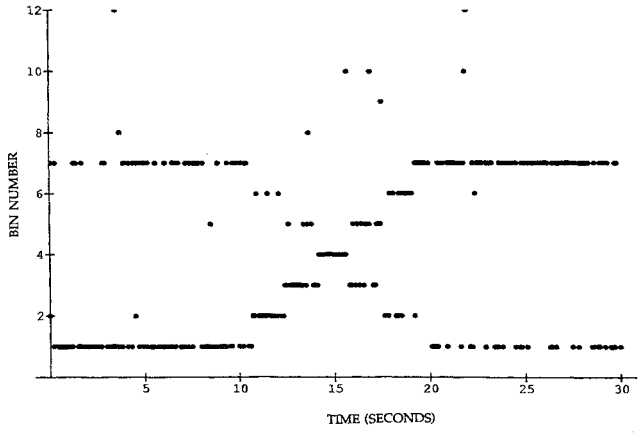

Fig. 3 Sample function of ostensible target orientation from the imager.

It is shown in Ref. 26 that the conditional mean of $\{\phi_t\}$ is generated by the equation involving just the $\{\vartheta_t\}$ process: between observations

$$\frac{\mathrm{d}}{\mathrm{d}t}\hat{\phi}_t = Q'\hat{\phi}_t \tag{9a}$$

and at an observation time

$$\Delta\hat{\phi} = \mathrm{var}(\phi_t)(\mathbf{1}_K \otimes \Delta\vartheta) \tag{9b}$$

where $\mathrm{var}(\phi_t) = \mathrm{diag}\hat{\phi}_t - \hat{\phi}_t\hat{\phi}_t'$. The KL vector $(\mathbf{1}_K \otimes \Delta\vartheta)$ simply repeats the L-dimensional process, $\{\Delta\vartheta_t\}$, K times. The observation is weighted in Eq. (9b) by the uncertainty in the estimation of the target regime. Thus, the dynamics of the upper link are delineated by a rather simple algorithm (9). Between image processor outputs, the image link extrapolates forward using the transition parameters, which describe the tempo of the encounter. When the imager classifies an image, the conditional distribution of the modal state is updated according to Eq. (9b). Equation (8) eliminates the secondary variable—orientation—and gives the lower dimensional estimate of turn rate. Note that in the LGM problem with time variable $\{A_t\}$, the covariance process $\{P_{xx}\}$ is deterministic. It is not the variability in the process dynamics per se, but rather the uncertainty in identifying $\{\omega_\psi\}$ that creates the need to adjust the filter bandwidth; $\{P_{xx}\}$ is random because $\{\omega_\psi\}$ is measured with delay and error. To the degree that $\{\sigma_t\}$ provides a more expeditious indication of the status of the maneuver process than does $\{y_t\}$, it is reasonable to assume that $\{P_{xx}\}$ is only weakly dependent on $\{y_t\}$ given $\{\sigma_t\}$. If the image quality is such as to make this approximation credible, it is possible to derive the equations for the conditional mean of the target location. This is achieved by applying the nonlinear filtering theorem as given in Ref. 1, Chap. 7, Proposition 4.1 repetitively for the necessary sequence of conditional moments. The general development is carried out in Ref. 27 and can be reduced to a simple form for this application. Define the gain-adaptive tracker EKF_A by the following algorithm (10–15): between observations

$$\mathrm{d}\hat{x}_t = \left(\textstyle\sum_i A_i[(P_{x\phi})_{\cdot i} + \hat{x}_t\hat{\phi}_i]\right)\mathrm{d}t \tag{10a}$$

at a location measurement

$$\Delta\hat{x}_t = P_{xx}D'(DP_{xx}D' + R_x)^{-1}\Delta\nu_x \tag{10b}$$

at an image measurement

$$\Delta\hat{x}_t = P_{x\phi}\Delta\vartheta \tag{10c}$$

Between observations the tracker extrapolates according to the best estimate of the state. The updates come as a complementary pair, location and image. The location update has a conventional form, and the image update involves increments in the $\{\vartheta_t\}$ process discussed earlier. Actually, there is a subtlety in Eqs. (10b) and (10c) because the second moments $\{P_{xx}\}$ and $\{P_{x\phi}\}$ must be computed. It is primarily in this calculation that EKF_A diverges from the more conventional extended Kalman filters: between observations

$$\frac{\mathrm{d}}{\mathrm{d}t}P_{xx} = \textstyle\sum_i A_i[\pi_{xx}(i) + P_{xx}\hat{\phi}_i + \hat{x}_t(P_{x\phi})'_{\cdot i}]$$

$$+ \textstyle\sum_i A_i[\pi_{xx}(i) + P_{xx}\hat{\phi}_i + \hat{x}_t(P_{x\phi})'_{\cdot i}]' + W \tag{11a}$$

at a location measurement

$$\Delta P_{xx} = -P_{xx}D'(DP_{xx}D' + R_x)^{-1}DP_{xx} \tag{11b}$$

at an image measurement

$$\Delta P_{xx} = -\Delta\hat{x}\Delta\hat{x}' + \textstyle\sum_k \pi_{xx}(k)\Delta\vartheta_k \tag{11c}$$

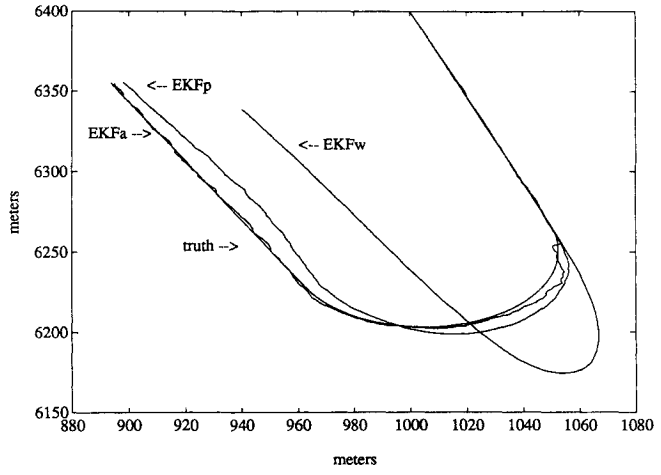

Fig. 4 Tracker performance in the plane.

Also between observations

$$\frac{\mathrm{d}}{\mathrm{d}t}P_{x\phi} = \sum_i A_i[\pi_{x\phi}(i) + P_{x\phi}\hat{\phi}_i' + \hat{x}_t(P_{\phi\phi})_{.i}'] + P_{x\phi}Q \tag{12a}$$

at a location measurement

$$\Delta P_{x\phi} = -P_{xx}D'(DP_{xx}D' + R_x)^{-1}DP_{x\phi} \tag{12b}$$

at an image measurement

$$\Delta P_{x\phi} = -\Delta\hat{x}\Delta\hat{\phi}' + \sum_k \pi_{x\phi}(k)\Delta\vartheta_k \tag{12c}$$

Equations (11) and (12) give the dynamics of the second error moments for this encounter. They contain two third-mixed moments: $\pi_{x\phi}(k) = E[(x - \hat{x})(\phi - \hat{\phi})'(\phi_k - \hat{\phi}_k) \mid Z_t]$ and $\pi_{xx}(k) = E[(x - \hat{x})(x - \hat{x})'(\phi_k - \hat{\phi}_k) \mid Z_t]$. The former can be calculated directly:

$$\pi_{x\phi}(m) = (P_{x\phi})_{.m}e_m' - \hat{\phi}_m P_{x\phi} - (P_{x\phi})_{.m}\hat{\phi}' \tag{13}$$

but the latter requires more care: between observations

$$\begin{aligned}\frac{\mathrm{d}}{\mathrm{d}t}\pi_{xx}(m) = {} & \sum_i \Big(A_i\{\Phi_i(m) + \hat{\phi}_i\pi_{xx}(m) \\ & + \hat{x}[\pi_{\phi x}(m)]_{i.} - (P_{x\phi})_{i.}(P_{\phi x})_{m.}\}\Big) + \sum_i \Big(A_i\{\Phi_i(m) \\ & + \hat{\phi}_i\pi_{xx}(m) + \hat{x}[\pi_{\phi x}(m)]_{i.} - (P_{x\phi})_{.i}(P_{\phi x})_{m.}\}\Big)' \\ & + \sum_j \pi_{xx}(j)Q_{jm}\end{aligned} \tag{14a}$$

at a location measurement

$$\begin{aligned}\Delta\pi_{xx}(m) = {} & -P_{xx}D'(DP_{xx}D' + R_x)^{-1}D\pi_{xx}(m) \\ & - [P_{xx}D'(DP_{xx}D' + R_x)^{-1}D\pi_{xx}(m)]'\end{aligned} \tag{14b}$$

at an image measurement

$$\begin{aligned}\Delta\pi_{xx}(m) = {} & -\Delta\hat{x}P_{\phi mx}^{+} - P_{x\phi m}^{+}\Delta\hat{x}' - P_{xx}^{+}\Delta\hat{\phi}_m \\ & - \Delta\hat{\phi}_m\Delta\hat{x}\Delta\hat{x}' + \sum_r \Phi_m(r)\Delta\vartheta_r\end{aligned} \tag{14c}$$

where $\Phi_m(r) = E[(x - \hat{x})(x - \hat{x})'(\phi_k - \hat{\phi}_k)(\phi_r - \hat{\phi}_r) \mid Z_t]$. [$P_{xx}^{+}$ is the updated value of P_{xx}, i.e., $P_{xx}^{+} = P_{xx}^{-} + \Delta P_{xx}$. The same designation is used for the other matrices in Eq. (14c)]. A direct calculation yields

$$\Phi_m(r) = (\delta_{rm} - \hat{\phi}_r)\pi_{xx}(m) - \hat{\phi}_m\pi_{xx}(r) + P_{xx}(\hat{\phi}_r\delta_{rm} - \hat{\phi}_r\hat{\phi}_m) \tag{15}$$

Although it might not be evident, a tedious but straightforward argument shows that if $\{A_i\}$ were independent of the maneuver index i, Eqs. (10–15) would reduce to Eqs. (3) and (4). In the case under consideration here, such a facile result does not hold, and all of the equations must be solved simultaneously. The filter equations are too convoluted to suggest online implementation on the current generation of microprocessors. To the degree that the approximations used in developing the algorithm are valid, the performance of EKF_A is of considerable interest because it represents essentially the best attainable from an image-enhanced tracker using the indicated architecture.

Image-Enhanced Performance

It is difficult to compare analytically the performance of EKF_A with the other trackers mentioned. Intuitively, it is reasonable to suppose that utilizing the cross moments of the location and the maneuver state would be advantageous, but it is not evident that the increased computation burden is justified. To illustrate the contrasts in performance, consider a specific vignette in which there is a ground borne target initially located at $(X_0, Y_0) = (6.4, 1.0)$ km, with initial velocity $(V_{x0}, V_{y0}) = (5.0, -13.3)$ m/s. Moving at constant velocity for $t \in [0, 10)$ s, a 0.5 g turn is made during $t \in [10, 20)$, after which the target returns to constant velocity motion. The omnidirectional accelerations will be assumed to be slight: $(\mathrm{d}w_x)^2 = (\mathrm{d}w_y)^2 = 0.01\ \mathrm{d}t\ (\mathrm{m/s^2})^2$. Figure 4 shows the target path (labeled truth) without the wide band acceleration.

Tracking will be accomplished with a 10 samples/s range-bearing sensor located at the origin with Gaussian errors of standard deviation 5.0 m and 0.25 deg, respectively, independent in time and type. This measurement specification suffices to determine the elemental EKF_w. The imager will be collocated and make measurements at the same rate; i.e., $\lambda = 10$ frames/s, placing the target in angular bins of width 30 deg (number of angular bins $L = 12$). To complete the measurement model, the imager errors must be quantified. A useful error taxonomy includes errors of three types: uniformly distributed errors (UDE), in which the output symbol is uniformly distributed without regard to the true orientation, 1.0% in toto; nearest neighbor errors (NNE), in which the output symbol is placed in the neighboring angular bin, 3.0% in toto; and projection error (PE), in which the output symbol places the target orientation in the bin situated symmetrically with respect to a line perpendicular to the line of sight, 29%. If the error categories are assumed to be independent in time and kind, the discernibility matrix can be deduced directly. Figure 3 shows a sample function of the output of such an imager in this trajectory, and the frequent PEs are a source of considerable uncertainty.

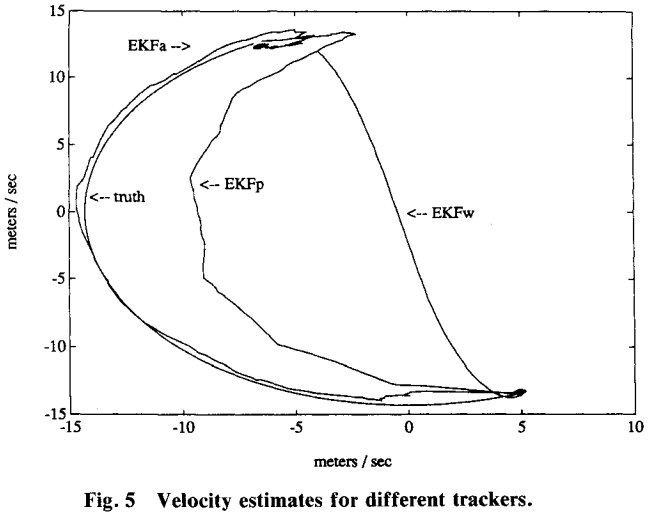

Fig. 5 Velocity estimates for different trackers.

To determine the processor dynamics in the upper link in Fig. 1, the tempo of the maneuver dynamics must be quantified. The lateral accelerations in the maneuver model will be given by a_1 = no turn, $a_2 = 17.3$ deg/s turn right, $a_3 = 17.3$ deg/s turn left, with the chain $\{\alpha_t\}$ symmetric about the coasting mode; i.e., the probabilistic character of $a_t = 2$ and 3 are identical. The elements of the q matrix are determined jointly by the mean sojourn times in each acceleration mode, $\{\nu_i, i = 1, 2, 3; \nu_2 = \nu_3\}$, and the transition probabilities from a maneuver to the nonmaneuvering mode. Let $q_1 = \mathcal{P}(\alpha_t = e_1 \mid \alpha_{t-} = e_2 \text{ and } \Delta\alpha_t \neq 0)$. Then q_1 measures the fraction of times that a maneuver ends in a coasting motion; e.g., $q_1 = 0$ implies pure jinking motion, and $q_1 = 1$ always interjects coasting between turns. Specifically, consider an encounter with the following tempo: $\nu_1 = 20$ s, $\nu_2 = 4$ s, $q_1 = 1.0$. Such a selection is in general correspondence with this rather benign scenario.

To see the effect of image-based gain adaptation consider three trackers: the conventional range-bearing algorithm EKF_W, a simple image-enhanced variant of the extended Kalman filter EKF_P, and the more sophisticated EKF_A described in the preceding section. The EKF_P is discussed in Refs. 28 and 29. As with the EKF_A, it uses Eq. (9) to translate image data into an estimate of $\{\alpha_t\}$. It adds the mean acceleration to the increments in the velocity estimates. To achieve higher gains during and soon after a turn, covariance modification is required. In the EKF_P, the process noise intensity W is augmented proportionally to acceleration uncertainty as measured by the variance of ω_ψ; an image-based pseudonoise is added to the target dynamics proportional to var $\omega_\psi = \Sigma_i a_i^2 \hat{\alpha}_i - (\Sigma_i a_i \hat{\alpha}_i)^2$. The corresponding value of $\{P_{xx}\}$ in EKF_P is the solution to Eq. (4) with the increased W. When the maneuver is resolvable from the image sequence ($\hat{\alpha}_t \cong e_i$), acceleration uncertainty is small. Alternatively, as the a posteriori probabilities of the maneuver hypotheses become more diffuse, var ω_ψ grows. Unfortunately, treating the maneuver as additive still obscures the geometric constraints in Eq. (5). Indeed, in the references it was found that EKF_P was quick to respond to a turn, but slow to return to quiescent operation during a subsequent coast. This was due to the failure of the gain augmentation to remain high long enough; var ω_ψ becomes small before the turn-induced errors are eradicated. To refine this adjustment, a more careful computation of the covariance process is necessary, and this computation is provided by the more sophisticated EKF_A.

Both the motion model and the observation equation are nonlinear. Furthermore, if the vignette is partitioned into pre-, post-, and maneuver coincident segments, the relative performance of the estimators changes as the target moves along its path. A good indication of performance can, however, be determined by simulation. Figure 4 shows the response of the

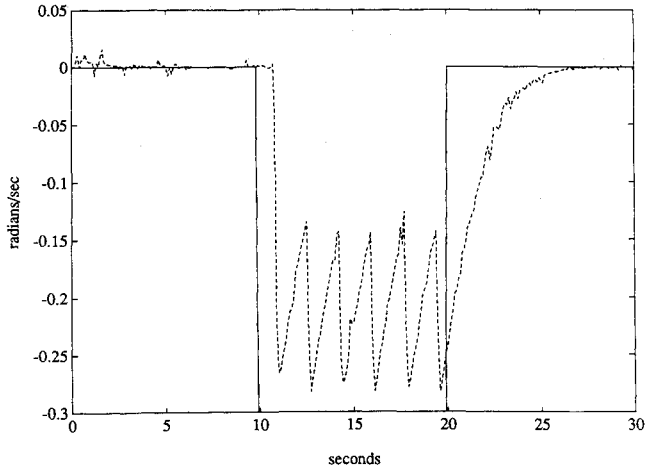

Fig. 6 Mean turn rate along with the true turn rate.

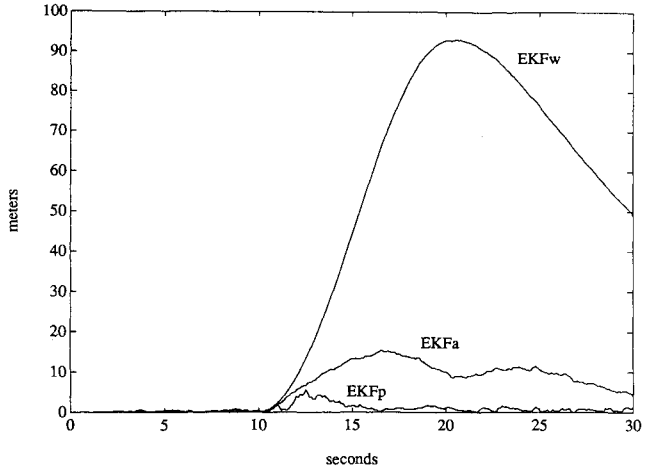

Fig. 7 Mean position error for the EKFs.

three trackers in the X-Y plane. To display biases, 20 trial mean sample paths are shown for each tracker rather than the (noisier) single sample paths. All of the filters perform well in the premaneuver phase, but EKF_W has considerable difficulty following a turn.

Figure 5 shows sample mean velocity profiles, and they are not as good. The reason for the clearly degraded velocity estimates is the fact that velocity is a slack variable in the estimation algorithm. It is included in the model, and the EKFs estimate its value concurrently with estimates of the location variables, but there is no direct velocity measurement. The filter tends to assign observation residuals to slack variables to a much greater degree than one might expect. This tendency is true to some extent during the nonmaneuvering phase $\omega_\psi = 0$, where the EKF_W model is valid, but the effect is magnified during a maneuver. In this phase of the scenario, there is conspicuous misidentification of the velocity, with EKF_W failing to recognize the correct sense of rotation. This poor performance in velocity is magnified by prediction algorithms, the simplest of which extrapolate to the predicted position along the direction of the velocity estimate.

Figures 4 and 5 show tracking performance in the plane, with time a parameter on the curve. It is difficult to gain a sense of the likelihood of loss of lock from these curves since loss of lock depends on the absolute error at concurrent times. Figures 6 and 7 show the mean turn rate generated by the image-based link $\{\hat{\alpha}_t\}$ and the time path of the mean position error. The image-enhanced trackers delay identifying the beginning of a maneuver because the target orientation must move across a portion of its coasting-resident bin and into an adjoining bin before the image interpreter senses that a path change is taking place. Once this signal is received, the upper link is quick to infer that a maneuver has begun. On the other hand, the identification of a transition back to a coasting mode is not nearly so decisive. A coasting mode is distinguished by a failure to move from bin to bin, and this is compatible, at least for several frames, with all of the maneuver hypotheses. For this reason, the maneuver estimate does not jump, but rather decays back to the coasting mode.

The sample mean position error is shown in Fig. 7. In the premaneuver phase of the encounter, all of the trackers are quite good, and if the scale were such as to show it, the EKF_W would be seen to be the best. In the maneuver-coincident phase, neglect of the turn causes large errors in the EKF_W with both image-enhanced trackers doing far better. In the postmaneuver phase, only EKF_A eliminates the residual error in an expeditious manner, the error in the EKF_P slowly decaying toward the quiescent level. It is this lingering deviation that makes evident how subtle gain selection is in a multimodal environment.

Both of the image-enhanced trackers have random gains; strictly speaking, EKF_W has a random gain as well since the

matrix D in Eq. (3) is obtained by linearizing the observation equation on the estimated path. Although interesting, displaying the gain process for each tracker would consume considerable space. To give a flavor of the variations between algorithms, it is worth looking at the behavior of one element of the error covariance matrix. Figure 8 shows the XX component of $\{P_{xx}\}$ for each of the three filters. This is but one component of the 4×4 matrix process, but it illustrates both the variability of the errors and the tendency of LGM filters to exaggerate their own performance. All of the filters have been initialized with a null error covariance.

Consider the EKF_W first. Because the omnidirectional noise is so small, the computed XX component of P_{xx} is small during the initial coast (which is opportune), but it is still small during the turn and thereafter (which is inopportune). The error variance is unaffected by the turn, and the ostensible standard deviation of the X error approaches 3 m. This inflates actual performance during the postmaneuver coast by more than an order of magnitude. This inability to recognize its own errors explains its degraded performance during the maneuver. The EKF_P is better because the residual uncertainty concerning a change in the turn rate keeps the gain higher than the EKF_W. Changes in the maneuver cause some change in $\{P_{xx}\}$ but they are neither large nor coincident with the precipitating event. Although more conservative than the EKF_W, the large position errors during a turn are not fully reflected in $\{P_{xx}\}$, as seen in Fig. 8, which shows computed standard deviation in X of 5 m, and in Fig. 7, which shows an error closer to 15 m.

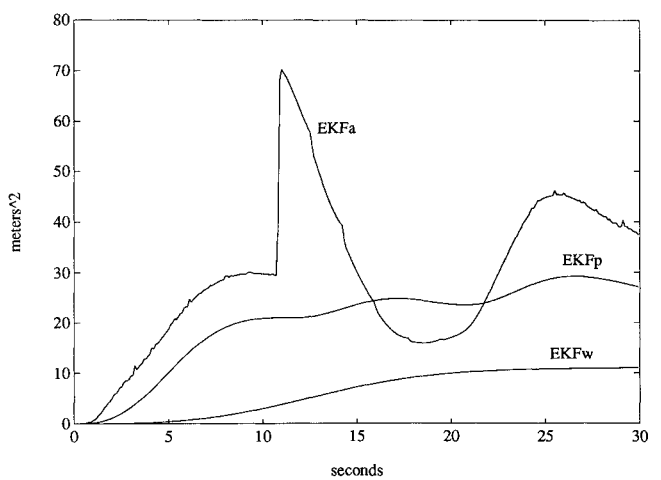

Fig. 8 The XX component of the error covariance for the three trackers.

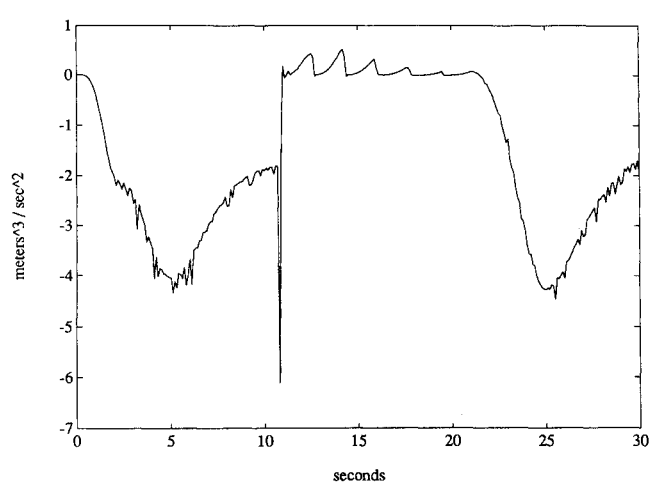

Fig. 9 Plot of $\pi_{xx}(\alpha_1)$ on the trajectory.

The behavior of the X error covariance in EKF_A is more responsive to the operating conditions. After the turn is recognized, the standard deviation in X builds almost immediately to 8.5 m, which is not out of line with the actual error. The immediacy of the change is created by the clear motion signal as evidenced by the change in $\{\hat{\phi}_t\}$. The error variance drops quickly during the sojourn in the turn, dropping below the computed variance for EKF_P. It quickly builds after the return to coast, but not as fast because the underlying transition cannot be as clearly distinguished. Note that the error variance retains the higher value for an extended period, thus maintaining a high bandwidth until the vestiges of the maneuver-induced residuals can be eliminated.

The calculation of the gains for EKF_A entails the solution to a set of stochastic differential equations. There are many individual moments, and their behavior will not be discussed here. It may, however, give some insight into the behavior of the estimator if at least one of the moments is displayed. Consider $\pi_{xx}(\alpha_1) = \Sigma_i E\{(X - \hat{X})(X - \hat{X})(\phi_i - \hat{\phi}_i) \mid Z_t\}$, where the sum is over all i corresponding to $\alpha = 1$ (the coasting mode). The sample mean path of $\pi_{xx}(\alpha_1)$ shown in Fig. 9 indicates how the $XX\alpha_1$ cross central moment changes as a function of the status of the encounter. To gain insight into the implications of the graph, note that the var X is smallest during a coast because the relatively long coasting sojourns permit higher accuracy in estimating the X-position coordinate. Intuitively, any shift from coast to a turn should cause var X to grow; i.e., the (random) var X is negatively correlated with the error in estimating α_1. This correlation is clearly seen to be the case in the distinguishable coasting intervals, e.g., [25, 30] s. During [11, 20] s, the probability of a coast is small. To the degree that it is thought that $\alpha_t = 1$, var X is reduced (after an appropriate delay as indicated in the decay after $t = 20$). The sharp change observed around $t = 11$ s is likely due to light damping of the design equations rather than some fundamental property of the moments.

Conclusions

This paper provides a new tracking algorithm for following an agile target. The focus here has been on creating a gain-adaptive filter based on an approximation to the comprehensive error covariance matrix. Through this intermediary, the linking of the regimes in a multimodal tracker can be made smoother. The tracking algorithm shown here is not seen as being implementable. Simply too many equations must be solved simultaneously for onboard synthesis. Nevertheless, the performance of the algorithm is important because it gives an indication of the latent quality of an image-enhanced tracker. There is work in progress on methods for reducing the computational burden on the system without simultaneously degrading performance effectiveness significantly.

Acknowledgments

This research was partially supported by a grant from the Hughes Aircraft Co., and by the MICRO Program of the State of California under Project 91-156.

References

[1]Wong, E., and Hajek, B., *Stochastic Processes in Engineering Systems*, Springer-Verlag, New York, 1985.

[2]Elliott, R. J., *Stochastic Calculus and Applications*, Springer-Verlag, New York, 1982.

[3]Gelb, A., *Applied Optimal Estimation*, MIT Press, Cambridge, MA, 1984.

[4]Maybeck, P. S., *Stochastic Models, Estimation, and Control*, Vols. 1, 2, and 3, Academic Press, New York, 1982.

[5]Cloutier, J. R., Evers, J. H., and Feeler, J. J., "Assessment of Air-to-Air Missile Guidance and Control Technology," *IEEE Control Systems Magazine*, Vol. 9, Oct. 1989, pp. 27-34.

[6]Speyer, J. L., Kim, K. D., and Tahk, M., "Passive Homing Missile Guidance Law Based on New Target Maneuver Models," *Journal of Guidance, Control, and Dynamics*, Vol. 13, No. 5, 1990, pp. 803-812.

[7]Williams, D. E., and Friedland, B., "Target Maneuver Detection

and Estimation," *Proceedings of the 27th IEEE Conference on Decision and Control*, Austin, TX, Dec. 1988, pp. 851–855.

[8]Sworder, D. D., Hutchins, R. G., and Kent, M., "The Utility of Imaging Sensors in Tracking Systems," *Automatica*, Vol. 29, No. 2, March 1993, pp. 445–449.

[9]Maybeck, P. S., and Stevens, R. D., "Reconfigurable Flight Control Via Multiple Model Adaptive Control Methods," *IEEE Transactions on Aerospace and Electronic Systems*, Vol. AES-27, May 1991, pp. 470–480.

[10]Blom, H. A. K., and Bar-Shalom, Y., "The Interacting Multiple Model Algorithm for Systems with Markovian Switching Coefficients," *IEEE Transactions on Automatic Control*, Vol. AC-33, Aug. 1988, pp. 780–783.

[11]Houles, A., and Bar-Shalom, Y., "Multisensor Tracking of a Maneuvering Target in Clutter," *IEEE Transactions on Aerospace and Electronic Systems*, Vol. AES-25, March 1989, pp. 176–188.

[12]Averbuch, A., Itzikowitz, S., and Kapon, T., "Radar Target Tracking Viterbi versus IMM," *IEEE Transactions on Aerospace and Electronic Systems*, Vol. AES-27, May 1991, pp. 550–563.

[13]Dufour, F., and Mariton, M., "Tracking a 3D Maneuvering Target with Passive Sensors," *IEEE Transactions on Aerospace and Electronic Systems*, Vol. AES-27, July 1991, pp. 725–739.

[14]Kendrick, J. D., Maybeck, P. S., and Reid, J. G., "Estimation of Aircraft Target Motion Using Orientation Measurements," *IEEE Transactions on Aerospace and Electronic Systems*, Vol. AES-17, March 1981, pp. 254–259.

[15]Moose, R. L., Vanlandingam, V. F., and McCabe, D. H., "Modeling and Estimation for Tracking Maneuvering Targets," *IEEE Transactions on Aerospace and Electronic Systems*, Vol. AES-15, May 1979, pp. 448–455.

[16]Ricker, G. G., and Williams, J. R., "Adaptive Tracking Filter for Maneuvering Targets," *IEEE Transactions on Aerospace and Electronic Systems*, Vol. AES-14, No. 1, 1978, pp. 185–193.

[17]Papoulis, A., *Probability, Random Variables and Stochastic Processes*, 3rd ed., McGraw-Hill, New York, 1991.

[18]Kim, K. D., Speyer, J. L., and Tahk, M., "Target Maneuvers Models for Tracking Estimators," *Proceedings of the IEEE International Conference on Control and Applications*, Paper RA-1-7, Jerusalem, April 1989.

[19]Bolger, P. L., "Tracking a Maneuvering Target Using Input Estimation," *IEEE Transactions on Aerospace and Electronic Systems*, Vol. AES-23, May 1987, pp. 298–310.

[20]Andrisani, D., Kim, E. T., Schierman, J., and Kuhl, F. P., "A Nonlinear Helicopter Tracker Using Attitude Measurements," *IEEE Transactions on Aerospace and Electronic Systems*, Vol. AES-27, Jan. 1991, pp. 40–47.

[21]Andrisani, D., and Schierman, J. D., "Tracking Maneuvering Helicopters Using Attitude and Rotor Angle Measurements," *Proceedings of the 21st Asilomar Conference on Circuits, Systems, and Computers* (Pacific Grove, CA), IEEE Service Center, Piscataway, NJ, Nov. 1987, pp. 328–333.

[22]Andrisani, D., Kuhl, F. P., and Gleason, D., "A Nonlinear Tracker Using Attitude Measurements," *IEEE Transactions on Aerospace and Electronic Systems*, Vol. AES-22, Sept. 1986, pp. 533–539.

[23]Lefas, C. C., "Using Roll Angle Measurements to Track Aircraft Maneuvers," *IEEE Transactions on Aerospace and Electronic Systems*, Vol. AES-20, No. 6, 1984, pp. 671–681.

[24]Brewer, J. W., "Kronecker Products and Matrix Calculus in Systems Theory," *IEEE Transactions on Circuits and Systems*, Vol. CAS-25, Sept. 1978, pp. 772–781.

[25]Sworder, D. D., and Hutchins, R. G., "Image-Enhanced Tracking," *IEEE Transactions on Aerospace and Electronic Systems*, Vol. AES-25, No. 5, 1989, pp. 701–710.

[26]Sworder, D. D., and Hutchins, R. G., "Maneuver Estimation Using Measurements of Orientation," *IEEE Transactions on Aerospace and Electronic Systems*, Vol. AES-26, No. 5, 1990, pp. 625–638.

[27]Sworder, D. D., and Haaland, K. S., "Algorithms for Design of Teleoperated Systems," *Control and Dynamic Systems, Advances in Theory and Applications*, Vol. 30, Pt. 3, Academic Press, New York, 1989, pp. 167–215.

[28]Hutchins, R. G., and Sworder, D. D., "Image Fusion Algorithms for Tracking Maneuvering Targets," *Journal of Guidance, Control, and Dynamics*, Vol. 15, No. 1, 1992, pp. 175–184.

[29]Sworder, D. D., and Hutchins, R. G., "Improved Tracking of an Agile Target," *Journal of Guidance, Control, and Dynamics*, Vol. 15, No. 5, 1992, pp. 1281–1284.